The role of an amino acid triad at the entrance of the heme pocket in human serum albumin for O_2 and CO binding to iron protoporphyrin IX†

Teruyuki Komatsu,*[a,b] Akito Nakagawa,[a] Stephen Curry,[c] Eishun Tsuchida,[a] Kenichi Murata,[d] Nobuhumi Nakamura[d] and Hiroyuki Ohno[d]

Received 19th May 2009, Accepted 29th June 2009
First published as an Advance Article on the web 22nd July 2009
DOI: 10.1039/b909794e

Complexation of iron(II) protoporphyrin IX (Fe^{2+}PP) into a genetically engineered heme pocket on recombinant human serum albumin (rHSA) creates an artificial hemoprotein which can bind O_2 reversibly at room temperature. Here we highlight a crucial role of a basic amino acid triad the entrance of the heme pocket in rHSA (Arg-114, His-146, Lys-190) for O_2 and CO binding to the prosthetic Fe^{2+}PP group. Replacing His-146 and/or Lys-190 with Arg resolved the structured heterogeneity of the possible two complexing modes of the porphyrin and afforded a single O_2 and CO binding affinity. Resonance Raman spectra show only one geometry of the axial His coordination to the central ferrous ion of the Fe^{2+}PP.

Introduction

Hemin [iron(III) protoporphyrin IX (Fe^{3+}PP), Fig. 1] dissociated from methemoglobin (metHb) is potentially toxic in the human body, because it intercalates in phospholipid membranes and participates in Fenton's reaction to produce hydroxyl radicals.[1] Hemopexin (Hpx, 60,000 Da), a β-glycoprotein in plasma (< 17 μM), captures the Fe^{3+}PP with an extraordinarily high binding affinity ($K > 10^{12}$ M^{-1}) and transports it to the liver for catabolism.[2] When Hpx becomes saturated (*e.g.* as a result of serious hemolytic injuries), the Fe^{3+}PP is first bound by human serum albumin (HSA, 66,500 Da) ($K = 1.1 \times 10^8$ M^{-1}),[3,4] the most abundant plasma protein (*ca.* 650 μM), and then transferred to Hpx. The biological function of the HSA–Fe^{3+}PP complex has attracted considerable interest for many years. However, Casella *et al.* reported little peroxidase or catalase activity,[5] so this naturally occurring hemoprotein may not play any significant role in vivo. If anything, HSA may serve to keep the incorporated hemin group physiologically silent.

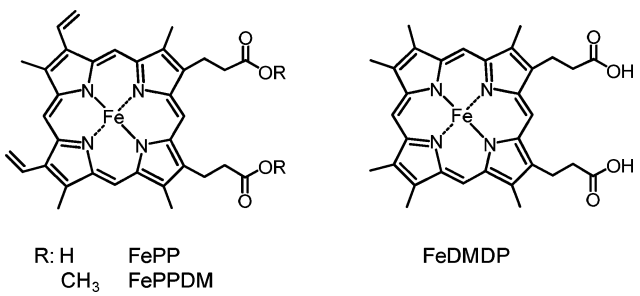

Fig. 1 Chemical formula of Fe porphyrins.

Crystal structure analysis of HSA–Fe^{3+}PP revealed that Fe^{3+}PP is bound within a deep hydrophobic slot in subdomain IB of HSA with axial coordination to the side-chain hydroxyl of Tyr-161 and salt bridges between the porphyrin propionates and a triad of basic amino acid residues at the pocket entrance (Arg-114, His-146, and Lys-190) (Fig. 2).[6,7] While the reduced ferrous HSA–Fe^{2+}PP is immediately autoxidized by O_2,[5] we found that a pair of site-specific mutations into the subdomain IB of HSA allows the Fe^{2+}PP to bind O_2: introduction of a proximal His at the Leu-185 position and substitution of the coordinated Tyr-161 with non-polar Leu (Y161L/L185H [rHSA**1**]) (Fig. 2).[9b,d] Remarkably, introduction of the proximal His at the Ile-142 position (on the opposite side of the porphyrin ring plane) also confers O_2 binding capability to the Fe^{2+}PP (I142H/Y161L [rHSA**2**]).[9a,c,d] These albumin O_2 transporters may serve as an effective red blood cell (RBC) substitute if the O_2 binding affinity is sufficient for clinical use. However, rHSA**1**–Fe^{2+}PP and rHSA**2**–Fe^{2+}PP both show two O_2 binding affinities ($P_{1/2}{}^{O2}$). The major component (species I, 60–75%) exhibits similar $P_{1/2}{}^{O2}$ to that of human RBC ($P_{1/2}{}^{O2} = 8$ Torr), but the minor component (species II, 25–40%) shows only a seventh to a tenth of the affinity (Table 1).[9] Our explanation for this observation is that the porphyrin plane of Fe^{2+}PP binds in the pocket in either of two alternative orientations (180° rotational isomers) that have slightly different geometries of axial His coordination to the central ferrous ion, only one of which confers high affinity O_2 binding.[9] Since less than 20% of species II of rHSA**2**–Fe^{2+}PP ($P_{1/2}{}^{O2} = 134$ Torr) is dioxygenated in the human lung's conditions ($P_{O2} = ca.$ 110 Torr, 37 °C), the low O_2 binding affinity component cannot effectively deliver O_2 to the tissues and should be excluded to develop this promising O_2 carrying plasma protein as an RBC substitute. Interestingly, a similar dependence of O_2 binding affinities on the orientations of the porphyrin ring

[a]*Research Institute for Science and Engineering, Waseda University, 3-4-1 Okubo, Shinjuku-ku, Tokyo, 169-8555, Japan. E-mail: teruyuki@waseda.jp; Fax: (+81) 3 5286 3148*
[b]*PRESTO, Japan Science and Technology Agency (JST), Japan. 4-1-8 Honcho, Kawaguchi-shi, Saitama, 332-0012, Japan*
[c]*Biophysics Section, Blackett Laboratory, Imperial College London, Exhibition Road, London, SW7 2AZ, United Kingdom*
[d]*Department of Biotechnology and Life Science, Tokyo University of Agriculture and Technology, 2-24-16, Naka-cho, Koganei-shi, Tokyo 184-8588, Japan*

† Electronic supplementary information (ESI) available: UV-vis absorption spectral data of rHSA–FePP and rHSA–FeDMDP, and absorption decay of CO rebinding to rHSA**2**–Fe^{2+}DMDP after laser flash photolysis. See DOI: 10.1039/b909794e

Table 1 O_2 and CO binding parameters of rHSA–Fe^{2+}PP in 50 mM potassium phosphate buffered solution (pH 7.0) at 22 °C

	k_{on}^{O2} ($\mu M^{-1}s^{-1}$)	k_{off}^{O2} (ms^{-1})		$P_{1/2}^{O2}$ (Torr)		k_{on}^{CO} ($\mu M^{-1}s^{-1}$)		k_{off}^{CO} (s^{-1})		$P_{1/2}^{CO}$ (Torr)	
		I	II	I	II	I	II	I	II	I	II
rHSA**1**–Fe^{2+}PP[a]	31	0.20	2.1	4	41	3.7	0.35	0.012	0.077	0.0026	0.18
rHSA**2**–Fe^{2+}PP[a]	7.5	0.22	1.7	18	134	2.0	0.27	0.013	0.079	0.0053	0.24
rHSA**1**(H146R)–Fe^{2+}PP	43	0.37	—	6	—	5.1	—	0.013	—	0.0033	—
rHSA**1**(L190R)–Fe^{2+}PP	24	0.35	—	9	—	4.0	—	0.010	—	0.0031	—
rHSA**1**(H146R/K190R)–Fe^{2+}PP	42	0.41	—	6	—	6.1	—	0.011	—	0.0022	—
rHSA**2**(H146R/K190R)–Fe^{2+}PP	11	0.30	—	17	—	1.7	—	0.012	—	0.0058	
Mb[b]	14	0.012		0.51		0.51		0.019		0.030	

[a] Ref. 9b. [b] Sperm whale Mb in 0.1 M potassium phosphate buffer (pH 7.0, 20 °C); ref. 17.

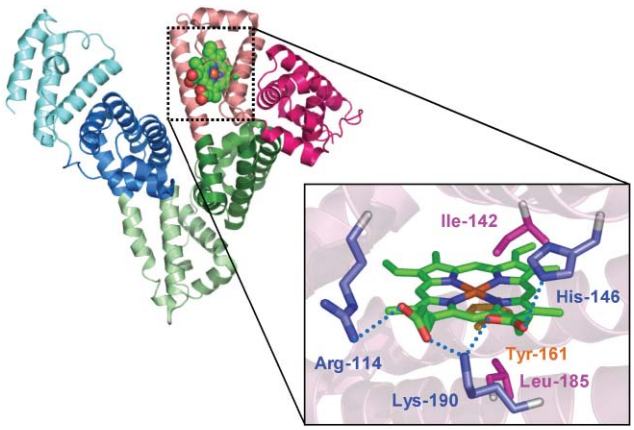

rHSA	Position				
	142	146	161	185	190
Wild type (WT)	Ile	His	Tyr	Leu	Lys
1	Ile	His	Leu	His	Lys
2	His	His	Leu	Leu	Lys
1(H146R)	Ile	Arg	Leu	His	Lys
1(K190R)	Ile	His	Leu	His	Arg
1(H146R/K190R)	Ile	Arg	Leu	His	Arg
2(H146R/K190R)	His	Arg	Leu	Leu	Arg

Fig. 2 Structure of the heme pocket in the rHSA(WT)–hemin complex (PDB ID: 1O9X from ref. 7).[8] Positions of the amino acids where site-specific mutations were introduced and abbreviations of the mutants are shown in the table.

plane is found in insect Hb.[10] If one could prepare a desired heme pocket architecture to distinguish the two possible binding modes of the asymmetric Fe^{2+}PP, it would provide new insights into the modulation of hemoprotein chemistry.

In this paper we report for the first time a role for the basic amino acid triad at the entrance of the heme pocket in rHSA in regulating O_2 and CO binding to the prosthetic Fe^{2+}PP group. Replacing His-146 and/or Lys-190 with Arg in rHSA**1**–Fe^{2+}PP and rHSA**2**–Fe^{2+}PP resolved the structural heterogeneity of the porphyrin plane orientation and afforded a single high-affinity O_2 and CO binding equilibrium. Moreover, the O_2 binding affinities of these hemoproteins are all similar to that of RBC. Resonance Raman (RR) spectra clearly show one geometry of the axial His coordination to Fe^{2+}PP.

Results and discussion

Design of the heme pocket

To bind the hemin molecule tightly, HSA exploits multiple electrostatic interactions between three basic amino acid residues and the hemin propionates at the wide entrance of the heme pocket (Fig. 2). Lys-190 adopts a central position and makes salt bridges to both propionic acid side chains. His-146 and Arg-114 provide a second electrostatic coordination with each carboxylate. Notably, the UV-vis absorption spectrum of HSA complexed with an iron(III) protoporphyrin IX dimethylester (Fe^{3+}PPDM, Fig. 1) showed very broad Soret and Q bands, suggesting that Fe^{3+}PPDM without peripheral carboxylic acids may not be bound stably within subdomain IB. This suggested that modification of this key basic amino acid triad involved in coordinating the hemin propionates could be used to regulate the orientation of the porphyrin ring plane in subdomain IB. We designed four new rHSA mutants based on the existing pair of double mutants that contain the substitutions necessary to confer O_2 binding to the Fe^{2+}PP (Y161L/L185H or I142H/Y161L).[9] His-146 and Lys-190 were replaced by more bulky and basic Arg: H146R, K190R, and H146R/K190R mutations were combined with the O_2 binding mutations (see Fig. 2 for details). We postulated that the introduction of Arg residues would reduce the space available at the entrance to the cavity and might thereby restrict the binding of Fe^{2+}PP to a single conformation.

Site-specific mutations were introduced into the HSA coding region in a plasmid vector (pHIL-D2 HSA). The proteins were expressed in the yeast species *Pichia pastoris*. The rHSA–Fe^{2+}PP complexes were prepared according to our previously reported procedures (see Experimental).

O_2 and CO binding properties of rHSA–Fe^{2+}PP

The UV-vis absorption spectra of all six rHSA(mutant)–Fe^{3+}PP were essentially identical (Fig. 3, Table S1†). They were easily reduced to the corresponding ferrous complexes by adding a small amount of degassed aqueous $Na_2S_2O_4$ under an N_2 atmosphere. A single broad absorption band (λ = 558–559 nm) in the visible region signified the formation of a five-*N*-coordinate high-spin complex similar to deoxy Mb[11] or the synthetic chelated heme in DMF.[12] The spectral features and amplitude did not change in the temperature range of 5–25 °C. These observations show that the guanidinium groups of Arg-146 or Arg-190 do *not* interact with

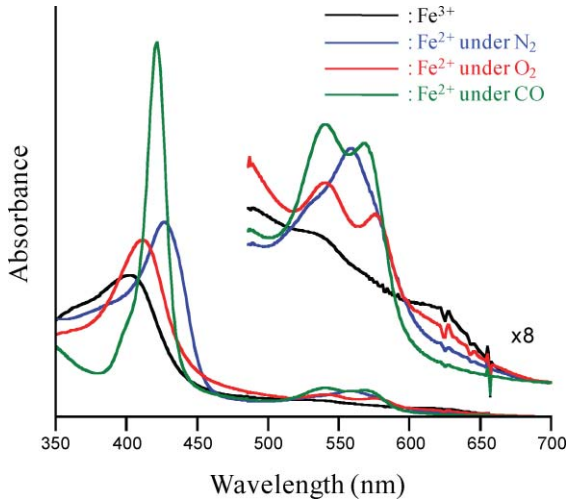

Fig. 3 UV-vis absorption spectral changes of rHSA**1**(H146R/K190R)–Fe^{2+}PP in 50 mM potassium phosphate buffered solution (pH 7.0) at 22 °C.

the ferrous iron of the Fe^{2+}PP, since the resulting formation of a six-*N*-coordinate low-spin complex would have yielded sharp and split α, β bands in the visible region[9c] and been sensitive to rapid oxidation by O_2 *via* an outer sphere mechanism.[13]

Upon exposure of the rHSA–Fe^{2+}PP solution to O_2 gas, the UV-vis absorption changed to that of the dioxygenated complex (Fig. 3).[9,11] After exposure to flowing CO, the Fe^{2+}PP produced a typical carbonyl complex.

We then used laser flash photolysis spectroscopy to determine association and dissociation rate constants (k_{on}, k_{off}) for O_2 and CO binding to rHSA–Fe^{2+}PP.[9] The time dependence of the absorption change accompanying the CO recombination to rHSA**1**–Fe^{2+}PP and rHSA**2**–Fe^{2+}PP obeyed double-exponentials, although the O_2 binding kinetics followed a single-exponential.[9] The slow phase (species II) of the CO rebinding showed 7–11-fold lower k_{on}^{CO} and 6-fold higher k_{off}^{CO} than those of the fast phase (species I) (Table 1). We interpreted this to mean that the low O_2 binding affinity conformers of rHSA**1**–Fe^{2+}PP and rHSA**2**–Fe^{2+}PP have bending strain in the proximal His coordination.[9,14–16] In contrast, the rebinding kinetics of O_2 and CO to rHSA**1**(H146R)–Fe^{2+}PP, rHSA**1**(K190R)–Fe^{2+}PP, rHSA**1**(H146R/K190R)–Fe^{2+}PP and rHSA**2**(H146R/K190R)–Fe^{2+}PP were strictly monophasic (Fig. 4). As a result, these hemoproteins showed single O_2 and CO binding affinity ($P_{1/2}^{O2}$ and $P_{1/2}^{CO}$), which were all similar to the higher affinities (species I) of the original double mutants (Table 1). We can conclude that the introduction of Arg into the entrance of the heme pocket of rHSA**1** and rHSA**2** is effective at excluding the low O_2 binding affinity conformer.

CO binding to rHSA–Fe^{2+}DMDP

To verify our interpretation that the replacement of H146 and/or K190 by Arg resolved the structural heterogeneity of the two complexing modes of the Fe^{2+}PP and gave a single O_2 and CO binding affinity, we examined the incorporation of a symmetrical iron(II) 2,4-dimethyl-deuteroporphyrin (Fe^{2+}DMDP, Fig. 1) as an active site. The UV-vis absorption spectrum of

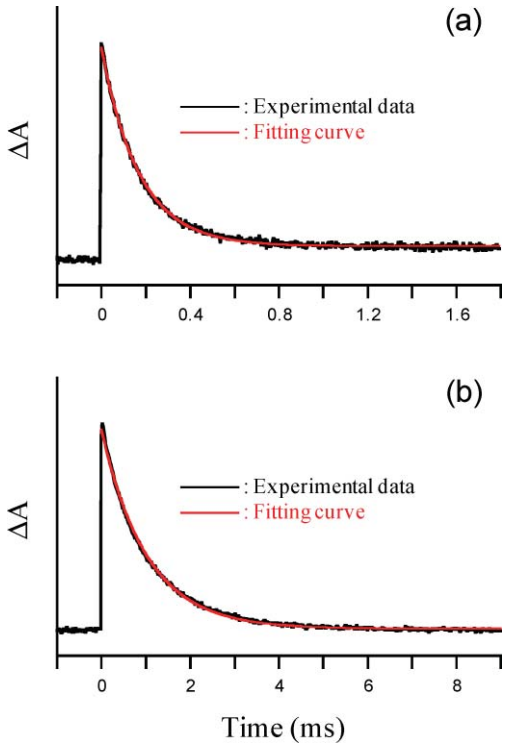

Fig. 4 Absorption decay of O_2 and CO rebinding to rHSA**1**(H146R/K190R)–Fe^{2+}PP after the laser flash photolysis at 22 °C; (a) O_2 and (b) CO. Both kinetics were composed of monophasic phases. A relaxation curve was fitted single exponential (red line).

the ferric rHSA**2**–Fe^{3+}DMDP showed a very similar pattern to that of rHSA**2**–Fe^{3+}PP though each λ_{max} value was hypsochromic (8–11 nm) shifted (Table S1†). The reduced ferrous form of rHSA**2**–Fe^{2+}DMDP under an N_2 atmosphere exhibited a slightly broadened Soret band absorption, but the main species was a five-*N*-coordinate high spin complex involving axial His-142 coordination. Upon introduction of O_2 gas through the solution, rHSA**2**–Fe^{2+}DMDP bound O_2 only at 5 °C and was observed to autoxidize at 22 °C. In general, the stability of the O_2 adduct complex of a heme derivative is sensitive to the electron density at Fe^{2+} and thus to the substituents at the porphyrin periphery.[18,19] Our attempt to determine the O_2 binding parameters of rHSA**2**–Fe^{2+}DMDP unfortunately failed. However, after introduction of CO gas, rHSA**2**–Fe^{2+}DMDP produced a stable carbonyl complex. We again used laser flash photolysis to characterize the CO binding properties of this hemoprotein. As expected, the absorption decay associated with CO recombination with rHSA**2**–Fe^{2+}DMDP was clearly monophasic (Fig. S1†). This result implied that the symmetric Fe^{2+}DMDP molecule is accommodated in subdomain IB of rHSA**2** in a single orientation and there is only one geometry of the axial His-142 coordination to the central ferrous ion of Fe^{2+}DMDP. Interestingly, the CO rebinding to rHSA**2**–Fe^{2+}DMDP (k_{on}^{CO}: 0.42 $\mu M^{-1}s^{-1}$) was relatively slow compared to that of rHSA**2**–Fe^{2+}PP and similar to Mb.[17]

RR and IR spectroscopies

The RR and infrared (IR) spectra of these artificial hemoproteins also supported the results described above. The stretching

frequencies of the carbonyl complex [ν(Fe–CO) and ν(CO)] provide crucial information about the Fe–trans ligand bond.[20,21] The high-frequency region of the RR spectra of rHSA**1**–Fe^{2+}PP(CO) and rHSA**1**(H146R/K190R)–Fe^{2+}PP(CO) both exhibited an intense peak at 1373 cm^{-1} (λ_{ex}: 413.1 nm), which indicates a deformed pyrrole-ring breathing-like mode (ν_4) and corresponds well to the value of the 6-coordinate low-spin carbonyl complex.[21a] However, while the low-frequency RR spectra of rHSA**1**–Fe^{2+}PP(CO) exhibited two ν(Fe–CO) bands at 493 and 525 cm^{-1}, rHSA**1**(H146R/K190R)–Fe^{2+}PP (CO) showed only a single ν(Fe–CO) band at 493 cm^{-1} (Fig. 5).[22] Since it is known that the weaker the Fe-trans ligand coordination, the stronger the Fe–CO bond in the carbonyl complex,[20] we assigned the higher 525 cm^{-1} band of rHSA**1**–Fe^{2+}PP(CO) to the low CO binding affinity conformer. The 493 cm^{-1} band was therefore assigned to the high affinity conformer, in which the proximal His-185 coordinates to the Fe^{2+}PP without unfavourable strain.

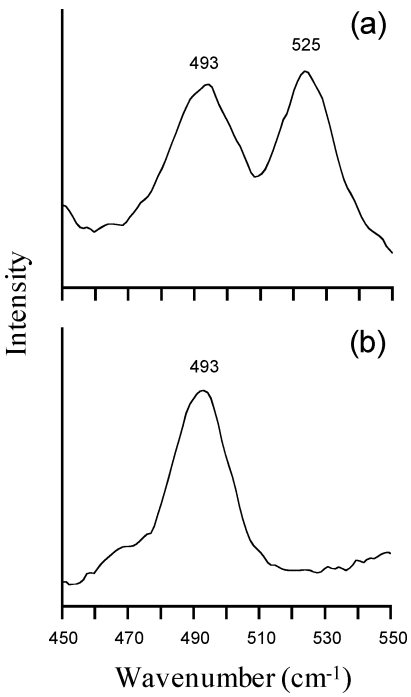

Fig. 5 Resonance Raman spectra of (a) rHSA**1**–Fe^{2+}PP(CO) and (b) rHSA**1**(H146R/K190R)–Fe^{2+}PP(CO) in 50 mM potassium phosphate buffered solution (pH 7.0) at 22 °C.

Regarding IR spectra, the ν(CO) vibration appeared at 1963 cm^{-1} for rHSA**1**–Fe^{2+}PP(CO) and at 1967 cm^{-1} for rHSA**1**(H146R/K190R)–Fe^{2+}PP(CO). Spiro *et al.* prepared a systematic plot of ν(Fe–CO) *versus* ν(CO) for a large number of carbonyl heme complexes and found a single inverse correlation when imidazole is the axial ligand.[21b,c] This is attributed to back donation of Fe^{2+} dπ electrons to the CO π* orbital. The relationship between ν(Fe–CO) and ν(CO) for rHSA**1**(H146R/K190R)–Fe^{2+}PP(CO) fits on the line for the imidazole complexes.[21b,c] On the other hand, the low O_2 binding component of rHSA**1**–Fe^{2+}PP(CO) showed a positive deviation from the line. This result again indicates a very weak electron donation from the proximal His-185 in the low O_2 binding conformer.

Conclusions

We prepared rHSA–Fe^{2+}PP complexes having a single O_2 and CO binding affinity by introducing Arg into the His-146 and/or Lys-190 positions. These artificial hemoproteins have a uniform Fe^{2+}PP orientation and His ligation (His-185 or His-142) geometry to the central ferrous ion without inclination. The key triad of the basic amino acid residues (Arg-114, His-146 and Lys-190) at the entrance of the heme pocket of HSA plays an important role in stabilizing the porphyrin molecule *via* salt-bridge formation and might also discriminate the two sides of the porphyrin ring. In mammals, His-146 is universally conserved, but Lys-190 is present only in primate albumin. The wild-type HSA statistically accommodates the hemin in alternative orientations; the discrimination of the porphyrin plane by serum albumin might be unnecessary for the evolution process. But the engineering of an rHSA–Fe^{2+}PP complex with a single O_2 binding affinity is potentially of tremendous clinical importance for blood substitutes and O_2-transporting therapeutic reagents.

Experimental

Materials and apparatus

All materials were used as purchased without further purification. Iron(III) protoporphyrin IX chloride (Fe^{3+}PP) was purchased from Fluka. Iron(III) protoporphyrin IX dimethyl ester chloride (Fe^{3+}PPDM) was synthesized from protoporphyrin IX dimethyl ester (Sigma). Iron(III) 2,4-dimethyl-deuteroporphyrin chloride (Fe^{3+}DMDP) was synthesized from 2,4-dimethyl-deuteroporphyrin dimethyl ester (Frontier Scientific).[23] UV-vis absorption spectra were obtained on an Agilent 8453 UV-visible spectrophotometer equipped with an Agilent 89090A temperature control unit. Kinetic measurements for the O_2 and CO bindings were carried out on a Unisoku TSP-1000WK time-resolved spectrophotometer with a Spectron Laser Systems SL803G-10 Q-switched Nd:YAG laser, which generated a second-harmonic (532 nm) pulse of 6-ns duration (10 Hz). A 150 W xenon arc lamp was used as the probe light source. The gas mixture with the desired partial pressure of O_2/CO/N_2 was prepared by a Kofloc Gasblender GB-3C. Resonance Raman spectra of the carbonyl rHSA–Fe^{2+}PP complexes were obtained on a JASCO NRS-1000 spectrophotometer using a Kaiser Optical Holographic Notch-Plus filter and a liquid N_2-cooled CCD detector. The excitation source was a Coherent Innova 90C Kr^+ laser. Infrared spectra of the carbonyl rHSA–Fe^{2+}PP complex were obtained on a JASCO FT/IR-4200 spectrophotometer.

Preparation of rHSA

The designed rHSAs were prepared according to our previously reported techniques.[9b] The mutations (H146R and/or K190R) were introduced into the rHSA coding region in a plasmid vector encoding the double mutant [rHSA**1** or rHSA**2**] by use of the Stratagene QuikChange mutagenesis kit. All mutations were confirmed by DNA sequencing. The plasmid was then digested by NotI and introduced into yeast (*Pichia pastoris* GS115) by electroporation. The expression protocols and media formulations were as previously described.[9b] The expressed proteins were harvested from the growth medium by precipitation with ammonium sulfate

and purified by a Cibacron Blue column of Blue Sepharose 6 Fast Flow (Amersham Pharmacia Biotech). After concentration using a Vivaspin 20 ultrafilter (10 kDa M_w cutoff), the samples were applied to a Superdex 75 column (Amersham Pharmacia Biotech) using 50 mM potassium phosphate as the running buffer. The purification steps were followed by SDS-PAGE analysis. The purified rHSA was lyophilized and stored in the freezer at –20 °C.

Preparation of rHSA–Fe^{2+}porphyrin

Typically 5 mL of 0.1 mM rHSA in 50 mM potassium phosphate (pH 7.0) was mixed with 0.8 mL of 0.688 mM Fe^{3+}PP in DMSO (Fe^{3+}PP : rHSA was molar ratio of 1:1) and incubated overnight with rotation in the dark at room temperature. The complex was then diluted with 50 mM potassium phosphate (*ca.* 15 mL) and concentrated to the initial volume (5.8 mL) using a Vivaspin 20 ultrafilter (10 kDa M_w cutoff). These dilution and concentration cycles were repeated to reduce the final concentration of DMSO to *ca.* <0.001 vol%. The rHSA–Fe^{2+}PPDM and rHSA–Fe^{2+}DMDP were also prepared in the same manner. The 50 mM phosphate buffered solution (pH 7.0) of rHSA–Fe^{3+}PP ([Fe^{3+}PP]: *ca.* 10 μM) in a 10 mm path length optical quartz cuvette sealed with a rubber septum was purged with N_2 for 30 min. A small excess amount of degassed aqueous sodium dithionite was added by microsyringe to the sample under an N_2 atmosphere to reduce the central ferric ion of the Fe^{3+}PP, generating the deoxy ferrous rHSA–Fe^{2+}PP.

Determination of O_2 and CO binding parameters

The O_2 and CO recombination with rHSA–Fe^{2+}PP after nanosecond laser flash photolysis of the dioxygenated or carbonyl complex occurs according to eqn (1) with the association rate constant (k_{on}^{L}) and dissociation rate constant (k_{off}^{L}) (where L: O_2 or CO).

$$Fe^{2+}PP\text{-}L \xrightarrow{h\nu} Fe^{2+}PP + L \underset{k_{off}^{L}}{\overset{k_{on}^{L}}{\rightleftharpoons}} Fe^{2+}PP\text{-}L \qquad (1)$$

$$[P_{1/2}{}^{L} = (K^{L})^{-1} = (k_{on}{}^{L}/k_{off}{}^{L})^{-1}]$$

The $k_{on}{}^{CO}$ was measured by following the absorption at 436 nm for Fe^{2+}PP(CO) or 411 nm for Fe^{2+}DMDP(CO) after laser pulse irradiation to the carbonyl complex at 22 °C. The $k_{on}{}^{O2}$ and O_2 binding equilibrium constant [$K^{O2} = (P_{1/2}{}^{O2})^{-1}$)] can be determined by a competitive rebinding technique by use of gas mixtures with different partial pressures of $O_2/CO/N_2$ at 22 °C. The relaxation curves that accompanied the O_2 or CO recombination were analyzed by single or double exponential profiles with Unisoku Spectroscopy & Kinetics software. The $k_{off}{}^{O2}$ was calculated from $k_{on}{}^{O2}/K^{O2}$. The $k_{off}{}^{CO}$ was measured by displacement with NO for the carbonyl complex at 22 °C. The time course of the UV-vis absorption change that accompanied the CO-dissociation was fitted to single or double exponential. The CO binding constants [$K^{CO} = (P_{1/2}{}^{CO})^{-1}$] were calculated from $k_{off}{}^{CO}/k_{on}{}^{CO}$.

Raman spectroscopy

Spectra of the carbonyl complexes of rHSA–Fe^{2+}PP ([Fe^{2+}PP]: 2–4 mM in 50 mM phosphate buffered solution (pH 7.0)) were collected using back-scattering geometry at an excitation wavelength of λ_{ex}: 413.1 nm. The laser power for the samples was 1.8 mW. Each spectrum was recorded with 20 s accumulation time at 22 °C, and ten repetitively measured spectra were averaged to improve the signal to noise ratio. Peak frequencies were calibrated relative to indene and CCl_4 as a standard and were accurate to 1 cm^{-1}.

IR spectroscopy

The IR spectra of the carbonyl complexes of rHSA–Fe^{2+}PP ([Fe^{2+}PP]: 2–4 mM in 50 mM phosphate buffered solution (pH 7.0)) were obtained in CaF_2 cells (JASCO, path length: 0.025 mm). The cell containing water was used for the reference. The spectrum was accumulated 64 times to improve its signal-to-noise ratio.

Acknowledgements

This work was partially supported by Grant-in-Aid for Scientific Research (No. 20750142, 20350058) from JSPS, PRESTO from JST, and Health Science Research Grants (Regulatory Science) from MHLW Japan.

Notes and references

1 V. Jeney, J. Balla, A. Yachie, G. M. Vercellotti, J. W. Eaton and G. Balla, *Blood*, 2002, **100**, 879.
2 E. Tolosano and F. Altruda, *DNA Cell Biol.*, 2002, **21**, 297.
3 T. Peters, *All about Albumin: Biochemistry, Genetics and Medical Applications*, Academic Press, San Diego, 1996, and references therein.
4 P. A. Adams and M. C. Berman, *Biochem. J.*, 1980, **191**, 95.
5 E. Monzani, B. Bonafe, A. Fallarrini, C. Redaelli, L. Casella, L. Minchiotti and M. Galliano, *Biochim. Biophys. Acta*, 2001, **1547**, 302.
6 M. Wardell, Z. Wang, J. X. Ho, J. Robert, F. Ruker, J. Ruble and D. C. Carter, *Biochem. Biophys. Res. Commun.*, 2002, **291**, 813.
7 P. A. Zunszain, J. Ghuman, T. Komatsu, E. Tsuchida and S. Curry, *BMC Struct. Biol.*, 2003, **3**, 6.
8 The picture was produced using PyMOL, W. L. DeLano, *The PyMOL Molecular Graphics System*, DeLano Scientific, San Carlos, CA, 2002.
9 (*a*) T. Komatsu, N. Ohmichi, P. A. Zunszain, S. Curry and E. Tsuchida, *J. Am. Chem. Soc.*, 2004, **126**, 14304; (*b*) T. Komatsu, N. Ohmichi, A. Nakagawa, P. A. Zunszain, S. Curry and E. Tsuchida, *J. Am. Chem. Soc.*, 2005, **127**, 15933; (*c*) T. Komatsu, A. Nakagawa, P. A. Zunszain, S. Curry and E. Tsuchida, *J. Am. Chem. Soc.*, 2007, **129**, 11286; (*d*) T. Komatsu, A. Nakagawa and E. Tsuchida, *Macromol. Symp.*, 2008, **270**, 187.
10 K. Gersonde, H. Sick, M. Overkamp, K. M. Smith and D. W. Parish, *Eur. J. Biochem.*, 1986, **157**, 393.
11 E. Antonini and M. Brunori, *Hemoglobin and Myoglobin in Their Reactions with Ligands*, North-Holland: Amsterdam, 1971, p 18.
12 T. G. Traylor, C. K. Chang, J. Geibel, A. Berzinis, T. Mincey and J. Cannon, *J. Am. Chem. Soc.*, 1979, **101**, 6716.
13 M. M. L. Chu, C. E. Castro and G. M. Hathaway, *Biochemistry*, 1978, **17**, 481.
14 From numerous investigations on synthetic model hemes, it has been shown that a bending strain in the proximal base coordination to the central Fe^{2+} atom, the "proximal-side steric effect", can increase the $k_{off}{}^{CO}$ and decrease $k_{on}{}^{CO}$, whereas it increases $k_{off}{}^{O2}$ without greatly altering the kinetics of O_2 association[14,15].
15 J. P. Collman, J. I. Brauman, B. L. Iverson, J. L. Sessler, R. M. Morris and Q. H. Gibson, *J. Am. Chem. Soc.*, 1983, **105**, 3052.
16 T. G. Traylor, S. Tsuchiya, D. Campbell, M. Mitchel, D. Stynes and N. Koga, *J. Am. Chem. Soc.*, 1985, **107**, 604.
17 R. Rohlfs, A. J. Mathews, T. E. Carver, J. S. Olson, B. A. Springer, K. D. Egeberg and S. G. Sligar, *J. Biol. Chem.*, 1990, **265**, 3168.
18 T. G. Traylor, D. K. White, D. H. Campbell and A. P. Berzinis, *J. Am. Chem. Soc.*, 1981, **103**, 4932.

19 A. Nakagawa, N. Ohmichi, T. Komatsu and E. Tsuchida, *Org. Biomol. Chem.*, 2004, **2**, 3108.
20 E. A. Kerr, H. C. Mackin and N.-T. Yu, *Biochemistry*, 1983, **22**, 4373.
21 (*a*) T. G. Spiro and J. M. Burke, *J. Am. Chem. Soc.*, 1976, **988**, 5482; (*b*) X.-Y. Li and T. G. Spiro, *J. Am. Chem. Soc.*, 1988, **110**, 6024; (*c*) K. M. Vogel, P. M. Kozlowski, M. Z. Zgierski and T. G. Spiro, *Inorg. Chim. Acta*, 2000, **297**, 11.
22 These peaks are not the stretching mode of a disulfide bond [ν(S–S)]. It is observed at 500–545 cm^{-1} in the Raman spectrum of protein (λ_{ex}: 532 nm). Although there are 17 S–S bridges in HSA, our spectra of rHSAs without heme exhibited no peak in that region. C. David, S. Foley, C. Mavon and M. Enescu, *Biopolymers*, 2008, **89**, 623.
23 K. M. Smith and L. A. Kehres, *J. Chem. Soc., Perkin Trans. 1*, 1983, 2329.